J Mater Sci: Mater Electron (2013) 24:4050–4059
DOI 10.1007/s10854-013-1360-6

Effect of solvents on the structural, optical and morphological properties of $Zn_{0.96}Cu_{0.04}O$ nanoparticles

M. Ashok kumar · S. Muthukumaran

Received: 26 March 2013 / Accepted: 25 June 2013 / Published online: 6 July 2013
© Springer Science+Business Media New York 2013

Abstract $Zn_{0.96}Cu_{0.04}O$ nanoparticles were synthesized by co-precipitation method using different solvents like ethanol, water and mixer of ethanol and water in 50:50 ratios. Crystalline phases and optical studies of the nanoparticles were studied by X-ray diffraction (XRD) and UV–visible photo-spectrometer. The XRD showed that the prepared nanoparticles have different microstructure without changing a hexagonal wurtzite structure. The calculated average crystalline size was high for ethanol (27.3 nm) due to the presence of more defects and low for water (26 nm) due to the reduction of defects and vacancies. The energy dispersive X-ray analyses confirmed the presence of Cu in ZnO system and the weight percentage is nearly equal to their nominal stoichiometry within the experimental error. The presence of lower Zn and Cu percentage in the sample prepared using ethanol than other solvents was due low reaction rate which was confirmed by XRD spectra. Water solvent has relatively stronger transmittance in the visible region which leads to the industrial applications especially in opto-electronic devices. The average crystalline size is slowly decreased from 27.3 nm (ethanol) to 26 nm (water) whereas energy gap is steadily increased from 3.56 eV (ethanol) to 3.655 eV (water) when water concentration is increased from 0 to 100 % in ethanol. Existence of functional groups and bonding were analyzed by FTIR spectra. The observed blue shift of UV emission from ethanol (349 nm) to water (340 nm) solution and the high I_{UV}/I_G ratio in water solution in photoluminescence spectra was due to the decrease of crystalline size and defects/secondary phases. The intensity of blue–green band emission was gradually decreased due to the reduction of defects and vacancies when water concentration is increased from 0 to 100 % in ethanol solution, which was consistent with the XRD observation.

M. Ashok kumar · S. Muthukumaran (✉)
PG and Research Department of Physics, H.H. The Rajah's College (Autonomous), Pudukkottai 622 001, Tamil Nadu, India
e-mail: drsmk123@yahoo.co.in

1 Introduction

ZnO is an important II–VI group semiconductor with wide and direct band gap (3.37 eV) [1] equivalent that of GaN [2]. Recently, ZnO has received much attention as a potential candidate material for solar energy conversion, storage devices, luminescence, electrostatic dissipative coatings, transparent UV protection films, chemical sensors, spintronic devices [3–5], antibacterial agent, photonic material [6], gas sensing [7], photo catalysts [8] etc. due to their unusual electrical, optical, mechanical and magnetic properties.

Doping of transition metal (TM) is an effective method to adjust the energy level surface states of ZnO, which can further improve by changing the doping concentrations and hence its physical, especially optical properties [9]. The most commonly used metallic dopants in ZnO based systems are Al, Co, Cu, Ga, Sn, etc. [10–14]. Among the different metallic doping elements, Cu is important because, (1) it is a prominent luminescence activator, which can modify the luminescence of ZnO crystals by creating localized impurity levels [15], (2) it has similar electronic shell structure, physical and chemical properties to those of Zn [16] and (3) it can change the microstructure and the optical properties of the ZnO system [12].

Different physical or chemical synthetic methods have been used to prepare the doped ZnO nanoparticles such as thermal decomposition, thermolysis [17], chemical vapour deposition, sol–gel [18], spray pyrolysis, precipitation [19],

vapour phase oxidation [20], thermal vapour transport, condensation [21], co-precipitation [22] and hydrothermal [23]. Among the different methods, the co-precipitation is one of the most important methods to prepare the nanoparticles. Co-precipitation is the name given by analytical chemists to a phenomenon whereby the fractional precipitation of a specified ion in a solution results in the precipitation not only of the target ion but also of other ions existing side by side in the solution.

Recently, Sharma et al. [24] have studied the doping dependent room temperature ferromagnetism (RTFM) and structural properties of $ZnO:Cu^{2+}$ nanorods. Cu-doped ZnO nanoparticles with 40 nm size have been synthesized by solution combustion method which showed a red shift and narrowing of band gap [25]. Cu-doped ZnO thin films annealing under oxygen atmosphere at 973 K for 2 h showed high UV luminous efficiency and good optical properties [26]. Recent first-principle calculations using density functional theory on Cu-doped ZnO showed a half metallic ground state and high ferromagnetic stability for Cu concentrations from 3.0 to 12.5 at% [27]. Initial doping of Cu into ZnO lattice increases the carrier concentration and the further doping of Cu would be expected to create a secondary phase (CuO) and thereby decrease the carrier concentration [28]. Since, Cu related phases like CuO are observed in primary lattice system at higher concentrations [29–32], in present investigation Cu doping concentration is limited to 0.04.

Even though lot of research work had been carried out on Cu-doped ZnO [29–35], the detailed study of solvent effect on structural, optical and morphological effect is still scanty. Solvents can influence reactions in a number of ways. Solvents may be used as a reaction medium to bring reactants together; as a reactant to react with a solute when it cannot be dissolved; as a carrier, to deliver chemical compounds in solutions to their point of use in the required amounts. Therefore, in present investigation, $Zn_{0.96}Cu_{0.04}O$ nanoparticles are synthesized by co-precipitation method using different solvents like ethanol, water and in 50:50 ratios. The effect of solvent on its structural, optical and morphological properties has been studied and discussed in detail.

2 Experimental procedure

2.1 Preparation of $Zn_{0.96}Cu_{0.04}O$ nanoparticles

For the synthesis of $Zn_{0.96}Cu_{0.04}O$ nanoparticles, the analytical grade (AR), high purity chemicals (Merc, >99 % purity) such as zinc nitrate hexahydrate ($Zn(NO_3)_2{\cdot}6H_2O$), copper (II) nitrate trihydrate ($Cu(NO_3)_2{\cdot}3H_2O$) and sodium hydroxide (NaOH) were used as precursors. Initially, appropriate amount of zinc nitrate hexahydrate and copper (II) nitrate trihydrate were dissolved in ethanol and kept stirring until get a clear solution. NaOH solution had been prepared separately by dissolving appropriate amount of NaOH in 50 ml ethanol. The prepared solution then added drop wise to the initial ethanol solution under constant stirring at room temperature and kept stirring for 2 h. The white and gelatinous precipitates were filtered and then washed several times to remove the impurities. The final precipitates were dried using an oven at 80 °C for 2 h. The dried precipitates were collected and grounded using an agate mortar. Finally, the synthesized nanoparticles were annealed at 500 °C in air atmosphere for 2 h followed by furnace cooling. The same procedure is repeated to the remaining solvents.

2.2 Characterization techniques

The crystal structure of $Zn_{0.96}Cu_{0.04}O$ nanoparticles with different solvents was determined by powder X-ray diffraction (XRD). XRD patterns were recorded by RigaKuC/max-2500 diffractometer using Cu Kα radiation ($\lambda = 1.5406$ Å) at 40 kV and 30 mA from $2\theta = 10°–80°$. The topological features and composition of Zn, O and Cu were determined by energy dispersive X-ray spectrometer on K and L lines. The surface morphology of $Zn_{0.96}Cu_{0.04}O$ nanoparticles were studied using a scanning electron microscope (SEM, JEOLJSM 6390). The UV–visible optical absorption study was carried out to explore their optical properties. The spectral absorption was determined using UV–visible spectrometer (Model: lambda 35, Make: Perkin Elmer) in the wavelength ranging from 300 to 500 nm at room temperature. The presence of chemical bonding in $Zn_{0.96}Cu_{0.04}O$ samples was studied by FTIR spectrometer (Model: Perkin Elmer, Make: Spectrum RX I) from 400 to 4,000 cm^{-1}. The sample used for this measurement is in the form of pellets prepared by mixing the nanoparticles with KBr at 2 wt%. The photoluminescence (PL) spectra of $Zn_{0.96}Cu_{0.04}O$ nanoparticles have been recorded between the wavelength ranging from 310 to 500 nm under the excitation of Xenon lamp laser with 315 nm line using a fluorescence spectrophotometer (F-2500) at room temperature.

3 Results and discussion

3.1 X-ray diffraction (XRD): structural studies

The typical XRD spectra of $Zn_{0.96}Cu_{0.04}O$ nanoparticles prepared in ethanol, water and in 50:50 ratios are shown in Fig. 1. The diffraction peaks of XRD spectra of $Zn_{0.96}Cu_{0.04}O$ nanoparticles prepared using ethanol as a solvent clearly shows the polycrystalline nature corresponding to the diffraction angles 31.61° (100), 34.27° (002), 36.10° (101),

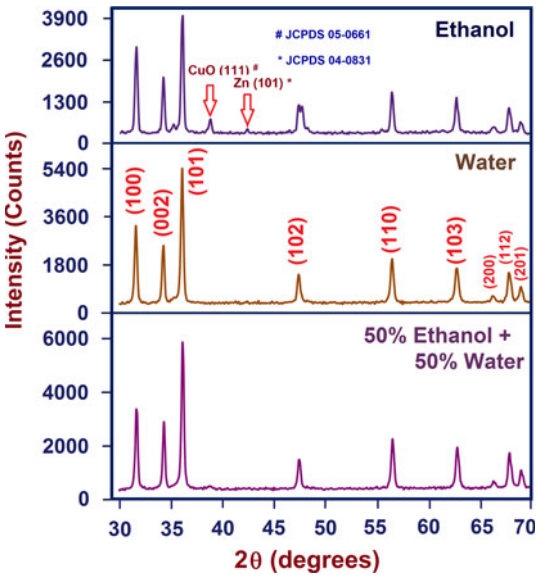

Fig. 1 Powder XRD pattern of $Zn_{0.96}Cu_{0.04}O$ nanoparticles for different solvents like ethanol, water and 50:50 ratios at room temperature

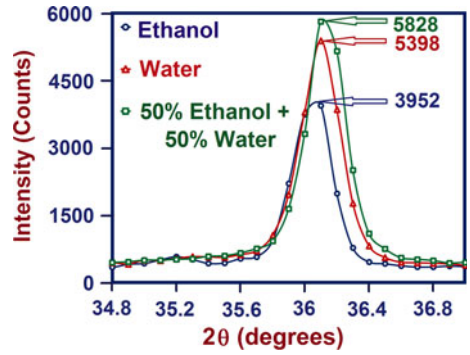

Fig. 2 The variation of peak position and peak intensity of $Zn_{0.96}Cu_{0.04}O$ nanoparticles for different solvents like ethanol, water and 50:50 ratios along (101) plane at room temperature

47.41° (102), 56.48° (110), 62.77° (103), 66.30° (200), 67.85° (112) and 68.99° (201) planes. The standard diffraction peaks show the crystal structure of $Zn_{0.96}Cu_{0.04}O$ nanoparticles is hexagonal wurtzite structure and very close to the standard data of pure ZnO (a = 3.2488 Å, c = 5.2061 Å, space group P63mc, 186, JCPDS data card No. 36-1451) with preferred orientation along (101) plane in all the samples. This is the most stable phase of ZnO. The existence of broad peaks indicates that the average crystalline size (D) is in the order of nano-meter scale. It is evident from the XRD spectra that there are no extra peaks corresponding to Cu, oxides of Cu or Cu related secondary and impurity phases for water and mixture of ethanol and water in 50:50 ratios, which may be attributed to the incorporation of Cu^{2+} into Zn^{2+} lattice site. But new phases at 38.73° and 42.33° are observed in XRD spectra of the nanoparticles prepared using ethanol as a solvent. The new phase at 38.73° in XRD spectra corresponds to CuO (111) (JCPDS card No. 05-0661). The presence of CuO phase may be due to the formation of CuO from remaining un-reacted Cu^{2+} ions [36]. The peak at 42.33° in the XRD spectra corresponding to Zn (101) (JCPDS card No. 04-0831) which may be due to the un-reacted Zn^{2+} ions. The presence of more un-reacted Cu^{2+} and Zn^{2+} ions in ethanol are due to its low polarity which reduces the interaction between precursor ions and surfaces of ZnO. Addition of high polarity water with ethanol reduces the un-reacted ions present in the solution, which leads to crystallization without any impurity phases. All the available reflections of the present XRD phases have been fitted with Gaussian distribution.

Even though, there is no considerable change in peak position (2θ), variation in peak intensities are noticeable for different solvents. The variation of peak intensity for different solvents along (101) plane is shown in Fig. 2. The nanoparticles prepared in the mixture of ethanol and water shows high peak intensity (5,828 counts), whereas the particles prepared in ethanol shows low intensity (3,952 counts) and water shows intermediate intensity (5,398 counts). The average crystalline size of the nanoparticles is calculated after appropriate background correction from X-ray line broadening of the diffraction peaks of (101) plane using Debye–Scherrer's formula [37],

$$\text{Average crystalline size (D)} = \frac{0.9\,\lambda}{\beta\cos\theta} \quad (1)$$

where, λ is the wavelength of X-ray used (1.5406 Å), β is the angular peak width at half maximum in radian along (101) plane and θ is Bragg's diffraction angle. The micro-strain (ε) can be calculated using the formula [38],

$$\text{Micro-strain } (\varepsilon) = \frac{\beta\cos\theta}{4}. \quad (2)$$

The size is minimum for water (26 nm) and maximum for ethanol (27.3 nm). The change of FWHM, peak intensity and average crystalline size may be due to the size or micro-strain or size and micro-strain [25, 39]. Table 1 shows the variation of FWHM value, average crystalline size (D) and micro-strain (ε) of $Zn_{0.96}Cu_{0.04}O$ nanoparticles for different solvents. The average crystalline size is decreased from 27.3 to 26 nm and the micro-strain is increased from 0.7755×10^{-3} to 0.8147×10^{-3} when water content in the ethanol is increasing from 0 to 100 %.

The growth of nanocrystallites with controlled shape and size as well as the organization of them into large 3-dimensional nanostructures is very important. ZnO is expected to crystallize by hydrolysis of Zn salts in a basic solution that can be formed using a strong or weak alkali. Zn^{2+} is known to coordinate in tetrahedral complexes. Depending on the given

Table 1 The variation of full width at half maximum (FWHM, β) value, average crystalline size (D) and micro-strain (ε) of $Zn_{0.96}Cu_{0.04}O$ nanoparticles for different solvents

Solvent	FWHM, β (degrees)	Average crystalline size, D (nm)	Micro-strain, ε (10^{-3})
Ethanol	0.306	27.3	0.7755
Ethanol + water (50:50)	0.3097	27.0	0.7852
Water	0.3214	26.0	0.8147

pH and temperature [40], Zn^{2+} is able to exist in a series of intermediates and ZnO can be formed by the dehydration of these intermediates. Chemical reactions in aqueous systems are usually considered to be in a reversible equilibrium and the driving force is the minimization of the free energy of the entire reaction system, which is the intrinsic nature of wet chemical methods [41]. When ZnO nucleus is newly formed owing to the high energy of the polar surfaces, the incoming precursor molecules tend to favorably adsorb on the polar surfaces. However, after adsorption of precursor molecules, the polar surface transforms into another polar surface with inverted polarity. For instance, Zn^{2+} terminated surface changes into an O^{2-} terminated surface, or vice versa. Such a process is repeated over time, leading to a fast growth. Furthermore, it has been suggested that Na^{+} which deliver from base NaOH is attracted by the OH^{-} and forms a virtual capping layer, thus, inhibiting the growth [42]. The detail reactions involved in the formation of ZnO [43] are,

$$Zn(NO_3)_2 + 2NaOH \leftrightarrow Zn(OH)_2 + 2NaNO_3 \text{(hydration)} \quad (3)$$

$$Zn(OH)_2 \leftrightarrow ZnO + H_2O \text{ (dehydration, ZnO formation)}. \quad (4)$$

The product is not necessarily $Zn(OH)_2$ but could also be in the form of $Zn(OH)^{+}$, $Zn(OH)_3^{-}$ or $Zn(OH)_4^{2-}$ depending on the parameters, such as the concentration of Zn^{2+} and the pH value (OH^{-}). All of these intermediate forms are actually in equilibrium, with the major forms being different under different reaction conditions [44]. Similar hydrolysis and dehydration process are involved in Cu simultaneously.

The growth of polar inorganic materials is sensitive to the reaction solvents and their morphologies. It could be tuned and controlled by the crystal–solvent interfacial interactions [45]. Relative growth rates can be readily tuned by varying the polarity of the solvents. Highly polar solvent molecules have stronger interactions with the polar surfaces of ZnO and settling down onto the polar surfaces by adsorbing from precursor molecules. Thus, solvents can be used as a reaction medium to bring reactants together and as a carrier. Lower solubility of pure ethanol leads to the presence of the less amount of $(OH)^{-1}$ which causes the reaction to precede much more slowly and hence the initial nucleus gets sufficient time to grow. Due to the slowness of the reactions the formation of nucleation centers also decreases. The production rate of $Zn(OH)_2$ and $Zn(OH)_4^{2-}$ units as well as the ZnO species is quite low. The slower growth rate causes the formation of large sized single crystals and induces the secondary phase formation and impurities which is reflected in the XRD spectra. In the ethanol–water system the presence of ethanol in equal amounts may reduce the reaction rate. The solubility of water is high. In the presence of the excess NaOH, the Zn-salt reacts vigorously to produce $Zn(OH)_2$ and. $Zn(OH)_4^{2-}$. These units decomposed to yield ZnO species, which agglomerated to form the nucleation center. The rapid formation of the ZnO species resulted in the faster growth of the ZnO nanostructures. Due to the rapid growth rate the probability of formation of the defect centers such as Zn interstitials, oxygen vacancy sites decreases.

Table 2 shows the peak position (2θ), d-value, cell parameters 'a' and 'c', c/a ratio, stress (σ), bond length and volume of $Zn_{0.96}Cu_{0.04}O$ nanoparticles for different solvents like ethanol, water and in 50:50 ratios. The small increase in cell parameters of $Zn_{0.96}Cu_{0.04}O$ nanoparticles compare to un-doped ZnO is due to the substitution of Cu in ZnO lattice [30, 46]. Bond length and volume of the $Zn_{0.96}Cu_{0.04}O$ nanoparticles are calculated from cell parameters by using Eqs. (3) and (4) and tabulated in Table 2. The Zn–O bond length has been calculated using the relationship [47],

$$\text{Bond length } (l) = \sqrt{\left(\frac{a^2}{3} + \left(\frac{1}{2} - u\right)^2 c^2\right)} \quad (5)$$

where, $u = a^2/3c^2 + 0.25$ is the potential parameter of the hexagonal structure. The volume of unit cell of hexagonal system has been calculated from the equation [48],

$$\text{Volume (V)} = 0.866 \times a^2 \times c. \quad (6)$$

The stress (σ) in the ZnO plans can be determined using the following expression [49],

$$\sigma = -233 \times 10^9((C_{bulk} - C)/C_{bulk}) \quad (7)$$

where, C is the lattice constant of ZnO plans calculated from XRD data, C_{bulk} is the strain-free lattice parameter of ZnO (5.2061 nm). The $Zn_{0.96}Cu_{0.04}O$ nanoparticles prepared in ethanol shows maximum stress, −1.5942 GPa and minimum stress (−0.9963 GPa) is observed at mixture of ethanol and water. The negative sign of stress indicates that the stress is tensile and the unit cells are under the state of compression. Normally, the total stress is originates from

Table 2 The variation of peak position (2θ), d-value, cell parameters 'a' and c, c/a ratio, stress (σ), bond length (*l*) and volume (V) of $Zn_{0.96}Cu_{0.04}O$ nanoparticles for different solvents

Solvent	Peak position, 2θ (degrees)	d-value (Å)	Cell parameters (Å)		c/a ratio	Stress, σ (GPa)	Bond length, I (Å)	Volume, V (Å)^3
			a = b	c				
Ethanol	36.02	2.6209	3.2721	5.2417	1.602	−1.5942	1.9913	48.6022
Ethanol + water (50:50)	36.10	2.6142	3.2660	5.2284	1.601	−0.9963	1.9871	48.2951
Water	36.07	2.6171	3.2688	5.2342	1.601	−1.2594	1.9890	48.4326

intrinsic and extrinsic stress. The intrinsic stress is associated with defects and impurities while the external stress is related to the lattice mismatch and thermal expansion. Wang et al. [50] noted that the growth along c-axis is retarded in the ethanol and Yan et al. [51] also proposed that the growth along c-axis suppressed in ethanol due to lagging of oxygen or hydroxyl OH^- ions in ethanol. Therefore, the higher tensile stress exhibited at ethanol may due to lattice mismatch or defects created along c-axis. The increase of crystalline size leads to more defects inside the lattice.

There is no considerable change in d-value, cell parameters, bond length, volume and peak position of the $Zn_{0.96}Cu_{0.04}O$ nanoparticles prepared using water and mixer of water and ethanol. The observed larger d-value, cell parameters, bond length and volume of $Zn_{0.96}Cu_{0.04}O$ nanoparticles prepared in ethanol (Table 2) is due to the presence of more defects compared to other solvents as discussed earlier. The observed constant c/a ratio revealing that there is no change in hexagonal wurtzite structure by solvents.

3.2 Scanning electron microscope (SEM) and energy dispersive X-ray (EDX) spectra

SEM is one of the promising techniques to study the surface morphology of the samples and it gives the important information regarding the growth mechanism, shape and size of the particles. The surface morphology of $Zn_{0.96}Cu_{0.04}O$ nanoparticles prepared at different solvents like ethanol, water and mixture of ethanol and water are shown in Fig. 3a, b, c, respectively. All the SEM micrographs clearly show that the average size of nanoparticles is in the order of nanometer. Figure 3a shows the synthesized nanoparticles using ethanol solvent are homogeneous and uniformly distributed throughout the structure. It has mixture of hexagon-like and spheroid-like particle structure in which hexagon-like structure is dominated with grain size around 15–40 nm. The mixture of spheroid-like, rod-like and the cluster form of uneven surface morphology are observed in $Zn_{0.96}Cu_{0.04}O$ nanoparticles prepared using water as in Fig. 3b. It is observed from Fig. 3b that the size of the particle get reduced and the particles are agglomerated each other with grain size around 10–30 nm. Figure 3c shows the well agglomerated and uniform spheroid-like particle structure around 10–38 nm. The existence of more defects greatly de-generates the particles size and shape which will make the greater particle size in ethanol than the other solvents. A good correlation is found to exist between mathematical calculations from XRD and SEM studies.

Chemical purity and stoichiometry of the samples were tested by EDX spectra. The typical EDX spectra of $Zn_{0.96}Cu_{0.04}O$ nanoparticles prepared in ethanol, water and in 50:50 ratios are as shown in Fig. 4. The quantitative atomic and weight percentage of the compositional elements such as Zn, Cu and O present in $Zn_{0.96}Cu_{0.04}O$ nanoparticles under different solvents are given in Table 3. The EDX analysis confirms the presence of Cu in ZnO and purity of system. It is observed from Fig. 4 that the weight percentage of Cu/Zn ratio is derived to be 4.56, 4.26 and 4.52 %, whereas atomic percentage is derived to be 4.54, 4.45 and 4.69 % for ethanol, water and 50:50 ratios, respectively. The calculated weight and atomic percentage are nearly equal to their nominal stoichiometry within the experimental error. The presence of lower Zn and Cu percentage in the sample prepared using ethanol than other solvents is due low reaction rate which is confirmed by XRD spectra.

3.3 UV–visible: optical studies

The UV–visible optical absorption spectra of $Zn_{0.96}Cu_{0.04}O$ nanoparticles prepared in various solutions like ethanol, water and in 50:50 ratios have been taken out at room temperature using UV–visible spectrometer (Model: Lambda 35, Make: Perkin Elmer) from 300 to 500 nm and are shown in Fig. 5. The insert of Fig. 5 shows the clear picture of the absorption changes from 300 to 370 nm. $Zn_{0.96}Cu_{0.04}O$ nanoparticles prepared using ethanol show high absorption than other solvents and $Zn_{0.96}Cu_{0.04}O$ nanoparticles prepared using water and mixture of ethanol and water in 50:50 ratios have more or less same absorption. The higher absorption in ethanol than other solvents may due to the presence of secondary phases/impurities.

The absorption peaks are shifted towards lower wavelength side from 324 to 318 nm when water concentration increasing from 0 to 100 % in the ethanol solution. A small absorption around 413 nm corresponding to CuO is noticed

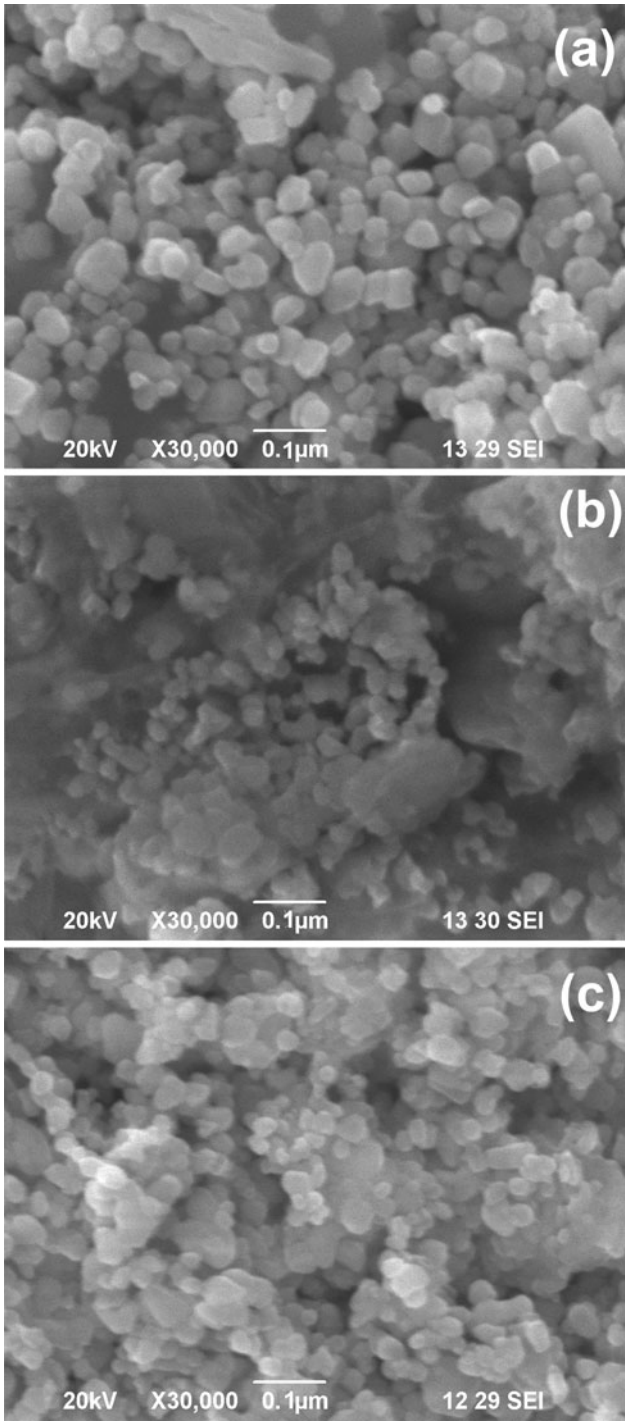

Fig. 3 Scanning electron microscope (SEM) images of $Zn_{0.96}Cu_{0.04}O$ nanoparticles for different solvents **a** ethanol, **b** water and **c** 50:50 ratios at room temperature

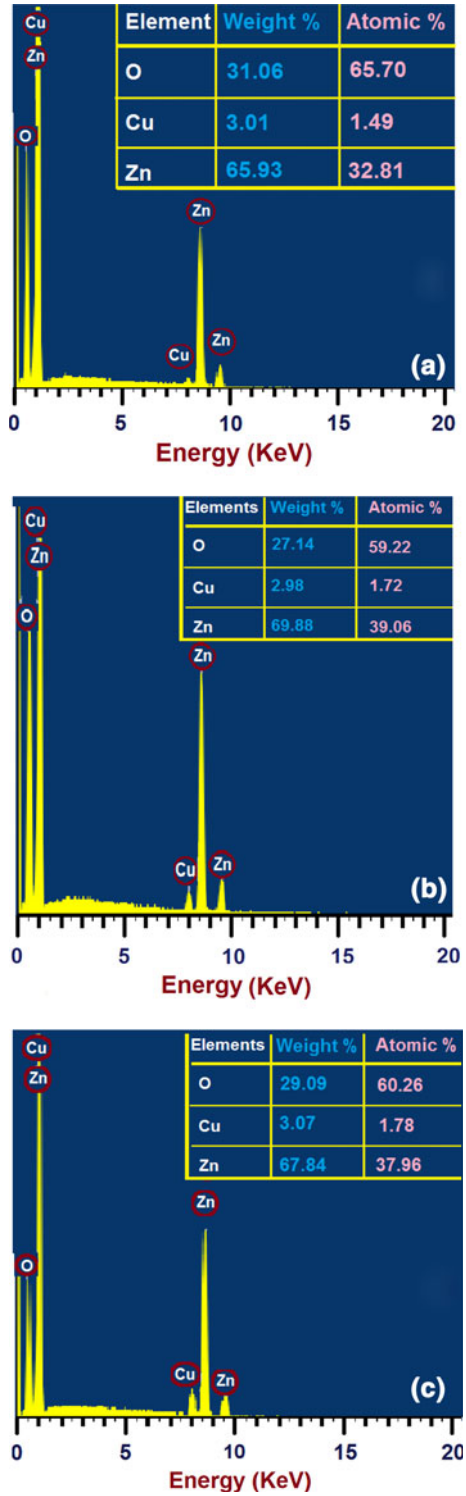

Fig. 4 Energy dispersive X-ray (EDX) spectra of $Zn_{0.96}Cu_{0.04}O$ nanoparticles for different solvents **a** ethanol, **b** water and **c** 50:50 ratios at room temperature. The *insert* shows the quantitative weight and atomic percentage of the compositional elements

for the $Zn_{0.96}Cu_{0.04}O$ nanoparticles prepared in ethanol solvent, which is supported by XRD spectra. The typical room temperature transmittance spectra of $Zn_{0.96}Cu_{0.04}O$ nanoparticles prepared in different solvents like ethanol, water and in 50:50 ratios are shown in Fig. 6. The insert of Fig. 6 shows the clear picture of transmittance changes from 300 to 370 nm. The transmission spectra of the $Zn_{0.96}Cu_{0.04}O$ nanoparticles show just opposite trend of the optical absorption spectra. Water solvent has a relatively stronger

Table 3 The quantitative analysis of the compositional elements present in $Zn_{0.96}Cu_{0.04}O$ nanoparticles for different solvents using EDX analysis

Solvents	Percentage of the elements (%)							
	Weight (%)			Cu/Zn ratio (%)	Atomic (%)			Cu/Zn ratio (%)
	Zn	O	Cu		Zn	O	Cu	
Ethanol	65.93	31.06	3.01	4.56	32.81	65.70	1.49	4.54
Ethanol + water (50:50)	67.84	29.09	3.07	4.52	37.96	60.26	1.78	4.69
Water	69.88	27.1	2.98	4.26	39.06	59.22	1.74	4.45

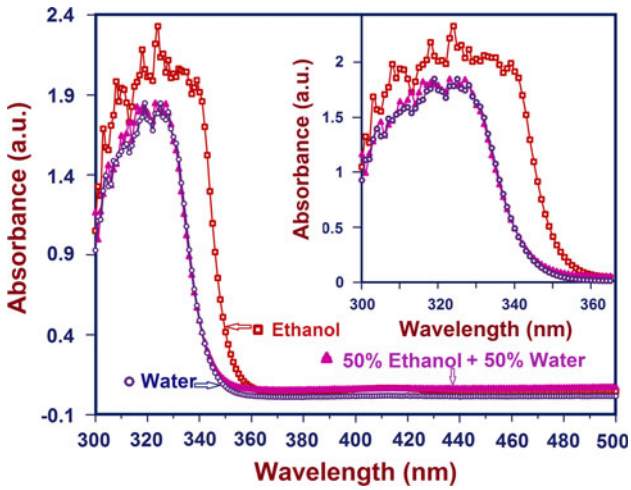

Fig. 5 UV–visible absorption spectra of $Zn_{0.96}Cu_{0.04}O$ nanoparticles for different solvents, ethanol, water and its 50:50 ratios as a function of wavelength from 300 to 500 nm. The *insert* shows the high resolution absorption spectra from 310 to 370 nm

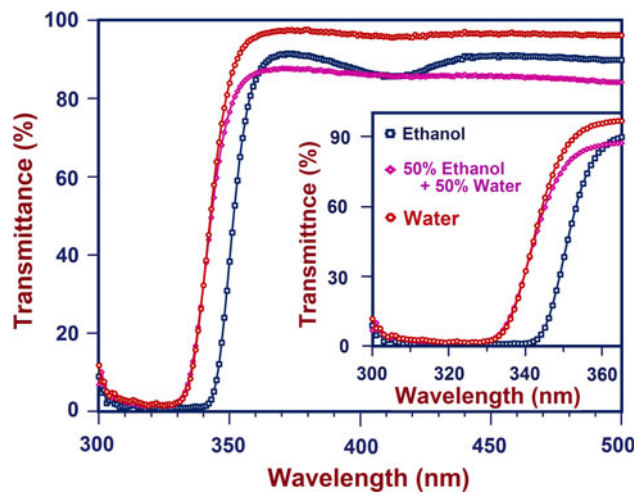

Fig. 6 Transmittance spectra of $Zn_{0.96}Cu_{0.04}O$ nanoparticles for different solvents, ethanol, water and its 50:50 ratios as a function of wavelength from 300 to 500 nm. The *insert* shows the high resolution absorption spectra from 310 to 370 nm

transmittance in the visible region compared to the other two samples synthesized in ethanol and ethanol–water mixed solvent. As ZnO is insoluble in water and ethanol, an appreciable amount of light gets scattered by dispersed particles owing to the higher transmittance in visible region [52]. In the visible region, the lower transmittance is observed for ethanol–water mixed solvent. Interestingly, the role of solvent in UV region is almost equal. The higher transmittance at water solution leads the sample to the industrial applications especially as transparent electrode.

The optical band gap is evaluated using the Tauc relation [53]:

$$h\upsilon = A\left(h\upsilon - E_g\right)^n \quad (8)$$

where, A as a constant, E_g is optical band gap of the material and the exponent n depends upon the type of transition. The values of n for direct allowed, indirect allowed and direct forbidden are 1/2, 2, 3/2. In the present case, n is taken as 1/2. The energy band gap of the $Zn_{0.96}Cu_{0.04}O$ nanoparticles are estimated by plotting $(\alpha h\upsilon)^2$ versus $h\upsilon$ as shown in Fig. 7. The extrapolation of the straight line to the energy ($h\upsilon$) axis gives the band gap of the material. The observed energy gap of $Zn_{0.96}Cu_{0.04}O$ nanoparticles using ethanol is minimum (3.56 eV) and it is maximum (3.655 eV) for water, whereas mixer of ethanol and water in 50:50 ratios has the intermediate value (3.64 eV). Wang et al. [54] discussed that both compositional and size effect are responsible for the band gap variation. They also noticed that the band gap is decreased with the increase of average crystalline size [54]. In the present work, the average crystalline size is slowly decreased from 27.3 nm (ethanol) to 26 nm (water) ($\Delta D \approx 1.3$ nm) whereas energy gap is steadily increased from 3.56 eV (ethanol) to 3.655 eV (water) when water concentration is increased from 0 to 100 % in ethanol as explained by Wang et al. [54].

3.4 FTIR studies

The band positions and numbers of absorption peaks are depending on crystalline structure, chemical composition and also on morphology [55]. FTIR is a technique used to obtain information about the chemical bonding in a material. It is used to identify the elemental constituents of a material. The characteristic peaks exhibited by FTIR

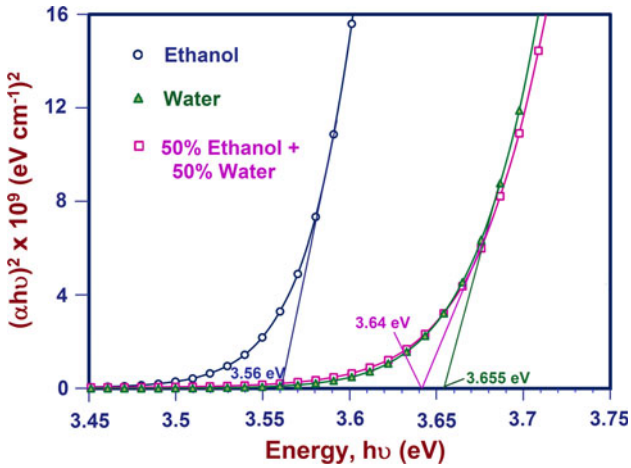

Fig. 7 The $(\alpha h\upsilon)^2$ versus $h\upsilon$ *curves* of $Zn_{0.96}Cu_{0.04}O$ nanoparticles for different solvents, ethanol, water and its 50:50 ratios for the optical energy gap calculation

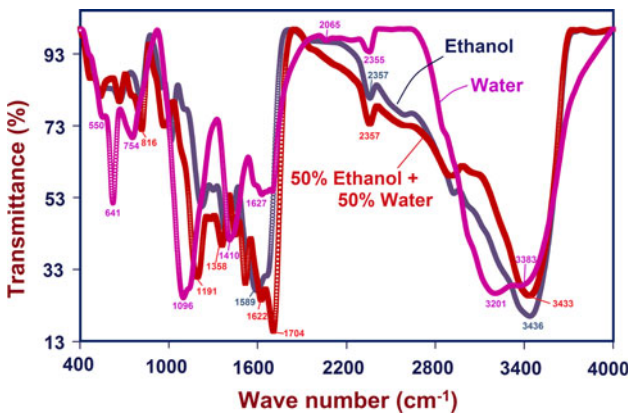

Fig. 8 FTIR spectra of $Zn_{0.96}Cu_{0.04}O$ nanoparticles for different solvents, ethanol, water and its 50:50 ratios at room temperature

spectra of $Zn_{0.96}Cu_{0.04}O$ nanoparticles prepared in various solutions like ethanol, water and in 50:50 ratios are shown in Fig. 8. The IR frequencies along with the vibrational assignments of the samples assigned at room temperature are listed in Table 4.

The main absorption bands at 3,436 and 1,193 cm^{-1} in the FTIR spectra of ethanol solution attributed to normal polymeric O–H stretching vibration of H_2O in Cu–Zn–O lattice [56]. These bands are shifted to 3,433 cm^{-1} and 1,191 cm^{-1} for a mixture of ethanol and water in 50:50 ratios; 3,383 cm^{-1} and 1,096 cm^{-1} for water solvent. Another sharp peak at 1,589 cm^{-1} in ethanol is attributed to H–O–H bending vibration, which is assigned to a small amount of H_2O in the ZnO nanoparticles [25]. It is shifted to higher wave number side (1,622 cm^{-1} at mixer of water and ethanol; 1,627 cm^{-1} at water). The absorption at 2,900 cm^{-1} are due C–H mode, which is absent in water solution and present on others. The absorption peak at 2,357 cm^{-1} is because of an existence of CO_2 molecule in air [57].

Table 4 IR peaks and their assignments of $Zn_{0.96}Cu_{0.04}O$ nanoparticles for different solvents

Assignments	Wave number (cm^{-1})		
	Ethanol	Ethanol + water	Water
O–H stretching vibration of H_2O	3,455	3,454	3,444
CN stretching vibration	2,122	2,132	2,132
H–O–H bending vibration	1,624	1,622	1,622
Stretching mode of Zn–O	638	652	660

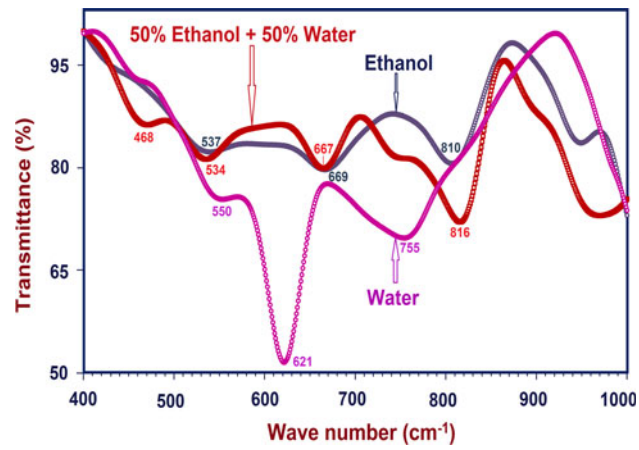

Fig. 9 The enlarged FTIR spectra of $Zn_{0.96}Cu_{0.04}O$ nanoparticles in the wave number range <1,000 cm^{-1} for different solvents, ethanol, water and its 50:50 ratios at room temperature

The characteristic IR peaks below 1,000 cm^{-1} is very important to study the presence or absence of Zn–O/Cu–O/Zn–O–Cu bonds and the functional groups. The enlarged spectrum in the wave number range <1,000 cm^{-1} is shown in Fig. 9. The medium to weak bands at 667 and 810 cm^{-1} in ethanol solution are assigned to the vibrational frequency of Zn–Cu–O local bond and defect states in Zn–Cu–O lattice [30]. The frequency at 810 cm^{-1} is shifted to 816 cm^{-1} for mixer of solution and 755 cm^{-1} for water solution. The change in intensity and FWHM corresponding to the frequency around 816–755 cm^{-1} represents a change in density of defect states surrounding to Cu^{2+} ions. The Zn–O bond is assigned to the stretching frequency at 537 cm^{-1} for ethanol solution which is shifted to lower frequency 534 cm^{-1} for mixer solution and shifted to higher frequency 550 cm^{-1} for water solution. The shift towards higher frequency side is due to the increase of Zn and Cu content in the system which is reflected by EDX spectra.

3.5 Photoluminescence (PL) studies

The correlation between structure and property is investigated by PL spectra which originate from the recombination

of the surface states [58]. The presence of defects such as electron–hole recombination centres and vacancies are responsible for optical absorption and emission spectra. The room temperature PL spectra of $Zn_{0.96}Cu_{0.04}O$ nanoparticles synthesized using pure ethanol, mixer of ethanol and water and water as a solvent at 315 nm excitation wavelength are shown in Fig. 10.

It is noticed from Fig. 10 that $Zn_{0.96}Cu_{0.04}O$ nanoparticles prepared by ethanol solution exhibit a strong near band (NB) ultra-violet (UV) emission centred at 349 nm (3.56 eV). The UV emission band is shifted to 341 nm (3.64 eV) by changing the solvent, mixer of water and ethanol solution; 340 nm (3.65 eV) for water solution. These results are consistent with the energy gap calculated from Fig. 7. The strong UV emission is originated from the excitonic recombination corresponding to the band edge emission of ZnO [59]. The presence of UV emission at room temperature demonstrates the high crystal quality of the Cu–ZnO crystals. The steady increase of intensity and the broadening of UV emission by the addition of water concentration in ethanol are due to the change in the crystal size and quality [60].

$Zn_{0.96}Cu_{0.04}O$ nanoparticles exhibit a weak defect related blue–green band (BGB) emission centred at 478 nm (2.56 eV). Even though, the intensity and the broadening are modulated by changing the solvent, there is no change in the peak intensity position of BGB emission. Generally, the origin of the green emission is referred to the deep level or trapped state emission. The BGB emission is associated with the intrinsic defect centers like oxygen vacancy (V_O), zinc vacancy (V_{Zn}), zinc interstitial (Zn_i) or oxygen interstitial (O_i) [61–63]. The BGB emission centred at 478 nm is also due to a radiative transition of an electron from the deep donar level of Zn_i to an acceptor level of neutral V_{Zn} [64]. The dominance of the green emission in the ethanol solution indicates that it exhibits a much higher defect concentration than the other solutions which is consistent with the XRD observation. The addition of Cu can effectively reduce the defects such as oxygen vacancies and zinc vacancies in ZnO nanocrystals [65]. The presence of higher Cu concentration and lower O concentration in water solution (as observed from EDX spectra) decreases the defects of O vacancies or O interstitials whereas ethanol solution has lower Cu concentration which leads to more defects and vacancies. The insert of Fig. 10 shows the I_{UV}/I_G ratio is gradually increased from ethanol to water solution and is maximum (1.968) for water which indicates that water solution has minimum defects and vacancies.

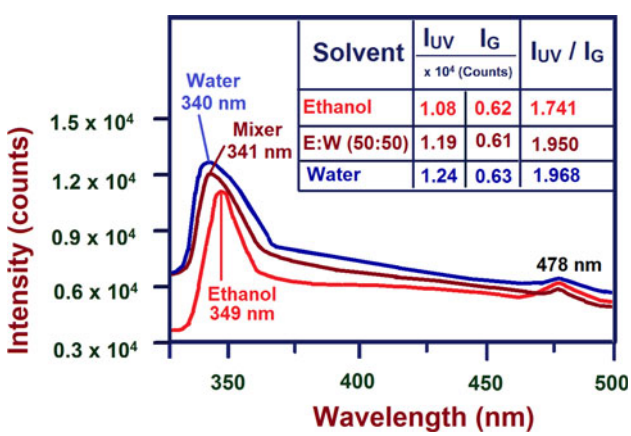

Fig. 10 Room-temperature PL spectra of $Zn_{0.96}Cu_{0.04}O$ nanoparticles for different solvents, ethanol, water and its 50:50 ratios using 315 nm line of Xe laser excitation source. The *insert* shows I_{UV}/I_G ratio for the different solvents

4 Conclusions

The following conclusions are drawn from the present investigation:

- $Zn_{0.96}Cu_{0.04}O$ nanoparticles are successfully synthesized by co-precipitation method using different solvents like ethanol, water and mixer of ethanol and water in 50:50 ratios.
- The XRD spectra showed that the prepared nanoparticles have different microstructure without changing a hexagonal wurtzite structure.
- The calculated average crystalline size is high for ethanol (27.3 nm) due to the presence of more defects and low for water (26 nm) due to the reduction of defects and vacancies which was confirmed by scanning electron microscope studies.
- The presence of lower Zn and Cu percentage in ethanol than other solvents is due low reaction rate which is confirmed by XRD spectra.
- Water solvent has a relatively stronger transmittance in the visible region which leads to the industrial applications especially for the preparation of opto-electronic devices.
- The average crystalline size is slowly decreased from 27.3 to 26 nm (water) whereas energy gap is steadily increased from 3.56 eV (ethanol) to 3.655 eV (water) when water concentration is increased from 0 to 100 % in ethanol.
- The observed blue shift of UV emission from ethanol (349 nm) to water (340 nm) solution and the high I_{UV}/I_G ratio in water solution in PL spectra is due to the decrease of crystalline size and defects/secondary phases.
- The intensity of blue–green band emission is gradually decreased when water concentration is increased from 0 to 100 % in ethanol solution; due to the reduction of defects and vacancies which is consistent with the XRD observation.

Acknowledgments The authors are thankful to the University Grant Commission (UGC), New Dehli, India, for financial support under the project [File no.: 41-968/2012 (SR)].

References

1. S. Singh, M.S.R. Rao, Phys Rev B **80**, 045210 (2009)
2. V.A. Karpina, V.I. Lazorenko, C.V. Lashkarev, V.D. Dobrowolski, L.I. Kopylova, V.A. Baturin, S.A. Lytuyn, V.P. Ovsyannikov, E.A. Mauvenko, Cryst Res Technol **39**, 980 (2004)
3. S.F. Pan, C. Song, X.J. Liu, Y.C. Yang, F. Zeng, Mater Sci Eng R **62**, 1 (2008)
4. N. Bai, T.Y. Tseng, J Appl Phys **74**, 695 (1993)
5. N.K. Zayer, R. Greef, K. Roger, A.J.C. Grellier, C.N. Pannell, Thin Solid Film **352**, 179 (1999)
6. J. Xie, H. Deng, Z.Q. Xu, Y. Li, J. Huang, J Cryst Growth **292**, 227 (2006)
7. C. Liewhiran, S. Phanichphant, Sensors **7**, 650 (2007)
8. L. Zi-Ling, D. Jian-Cheng, D. Jing-Jing, L. Fei-Fei, Mater Sci Eng B **150**, 99 (2008)
9. M. Sima, I. Enculescu, M. Sima, M. Enache, E. Vasile, J.P. Ansermet, Phys Stat Solidi B **244**, 1522 (2007)
10. J.J. Ding, H.X. Chen, X.G. Zhao, S.Y. Ma, J Phys Chem Solids **71**, 346 (2010)
11. Z.Q. Ma, W.G. Zhao, Y. Wang, Thin Solid Films **515**, 8611 (2007)
12. Z. Zhang, J.B. Yi, J. Ding, L.M. Wong, H.L. Seng, S.J. Wang, J.G. Tao, G.P. Li, G.Z. Xing, T.C. Sum, C.H.A. Huan, T. Wu, J Phys Chem C **112**, 9579 (2008)
13. J. Zhong, S. Muthukumar, Y. Chen, Y. Lu, Appl Phys Lett **83**, 3401 (2003)
14. T. Yamada, A. Miyake, S. Kishimoto, H. Makino, N. Yamamoto, T. Yamamoto, Surf Coat Technol **202**, 973 (2007)
15. Y.M. Tao, S.Y. Ma, H.X. Chen, J.X. Meng, L.L. Hou, Y.F. Jia, X.R. Shang, Vacuum **85**, 744 (2011)
16. Z.B. Bahsi, A. Yavuz Oral, Opt Mater **29**, 672 (2007)
17. M.S. Niasari, F. Davar, A. Khansari, J Alloys Compd **509**, 61 (2011)
18. J. Yang, L. Fei, H. Liu, Y. Liu, M. Gao, Y. Zhang, L. Yang, J Alloys Compd **509**, 3672 (2011)
19. Y. Yang, H. Chen, B. Zhao, X. Bao, J Cryst Growth **263**, 447 (2004)
20. J.Q. Hu, Q. Li, N.B. Wong, C.S. Lee, S.T. Lee, Chem Mater **14**, 1216 (2002)
21. J.Y. Lao, J.Y. Huang, D.Z. Wang, Z.F. Ren, Nano Lett **3**, 235 (2003)
22. R. Chauhan, A. Kumar, R.P. Chaudharya, J Chem Pharm Res **2**, 178 (2010)
23. R. Savu, R. Parra, E. Joanni, B. Jancar, S.A. Elizario, R. de Camargo, P.R. Bueno, J.A. Varela, E. Longo, M.A. Zaghate, J Cryst Growth **311**, 4102 (2009)
24. P.K. Sharma, R.K. Dutta, A.C. Pandey, J Magn Magn Mater **321**, 4001 (2009)
25. A. Jagannatha Reddy, M.K. Kokila, H. Nagabhushan, R.P.S. Chakradhar, C. Shivakumar, J.L. Rao, B.M. Nagabhushan, J Alloys Compd **509**, 5349 (2011)
26. D. Wang, J. Zhou, G. Liu, J Alloys Compd **487**, 545 (2009)
27. L.M. Huang, A.L. Rosa, R. Ahuja, Phys Rev B **74**, 075206 (2006)
28. Y. Wei, D. Hou, S. Qiao, C. Zhen, G. Tang, Phys B **404**, 2486 (2009)
29. L.-H. Ye, A.J. Freeman, B. Delley, Phys Rev B **73**, 033203 (2006)
30. S. Muthukumaran, R. Gopalakrishnan, Opt Mater **34**, 1946 (2012)
31. M. Ferhat, A. Zaoui, R. Ahuja, Appl Phys Lett **94**, 142502 (2009)
32. H. Liu, J. Yang, Z. Hua, Y. Zhang, L. Yang, L. Xiao, Z. Xie, Appl Surf Sci **256**, 4162 (2010)
33. Y.S. Sonawane, K.G. Kanade, B.B. Kale, R.C. Aiyer, Mater Res Bull **43**, 2719 (2008)
34. O. Lupan, T. Pauporté, T.L. Bahers, B. Viana, I. Ciofini, Adv Funct Mater **21**, 3564 (2011)
35. T.S. Herng, S.P. Lau, S.F. Yu, S.H. Tsang, K.S. Teng, J.S. Chen, J Appl Phys **104**, 103104 (2008)
36. P.K. Sharma, M. Kumar, A.C. Pandey, J Nanopart Res **13**, 1629 (2011)
37. S. Muthukumaran, R. Gopalakrishnan, Phys B **407**, 3450 (2012)
38. P.P. Hankare, P.A. Chate, D.J. Sathe, P.A. Chavan, V.M. Bhuse, J Mater Sci Mater Electron **20**, 374 (2009)
39. J. Pelleg, E. Elish, J Vac Sci Technol **A20**, 754 (2002)
40. S. Baruah, J. Dutta, J Cryst Growth **311**, 2549 (2009)
41. S. Xu, Y. Shen, Y. Ding, Z.L. Wang, Adv Funct Mater **20**, 1493 (2010)
42. R. Viswanath, H. Amenitsch, D.D. Sarma, J Am Chem Soc **129**, 4470 (2007)
43. S.B. Rana, P. Singh, A.K. Sharma, A.W. Carbonari, R. Dogra, J. Optoelect, Adv Mater **12**, 257 (2010)
44. S. Yamabi, H. Imai, J Mater Chem **12**, 3773 (2002)
45. B. Cheng, E.T. Samulski, Chem Commun **3**, 986 (2004)
46. R. Elilarassi, G. Chandrasekaran, J Mater Sci Mater Electron **21**, 1169 (2010)
47. B.D. Cullity, *Elements of X-ray diffractions* (Addison-Wesley, Reading, 1978)
48. G. Srinivasan, R.T.R. Kumar, J. Kumar, J Sol–Gel Sci Technol **43**, 171 (2007)
49. O. Lupan, T. Pauporte, L. Chow, B. Viana, F. Pelle, L.K. Ono, B.R. Cuenya, H. Heinrich, Appl Surf Sci **256**, 1895 (2010)
50. M. Wang, E.J. Kim, S.H. Hahn, C. Park, K.K. Koo, Cryst Growth Design **8**, 501 (2008)
51. L. Yan, L. Chuan-sheng, Trans Nonferrous Meter Soc China **19**, 399 (2009)
52. T. Ghoshal, S. Kar, S. Chaudhuri, J. Crys, Growth **293**, 438 (2006)
53. S. Muthukumaran, M. Ashok Kumar, J Mater Sci Mater Electron **23**, 811 (2012)
54. Y. Wang, G. Ouyang, L.L. Wang, L.M. Tang, D.S. Tang, C.Q. Sun, Chem Phys Lett **463**, 383 (2008)
55. Z. Yang, Z. Ye, Z. Xu, B. Zhao, Phys E **42**, 116 (2009)
56. K. Nakamoto, *Infrared and Raman spectra of inorganic and coordination compounds, Parts-A and B* (Wiley, New York, 1997)
57. M. Arshad, A. Azam, A.S. Ahmea, S. Mollah, A.H. Naqvi, J Alloys Compd **509**, 8378 (2011)
58. N. Chestony, T.D. Harris, R. Hull, L.E. Brus, J Phys Chem **90**, 3393 (1986)
59. C.K. Xu, K.K. Yang, Y.Y. Liu, L.W. Huang, H. Lee, J. Cho, H. Wang, J Phys Chem C **112**, 19236 (2008)
60. T. Yamamoto, H. Katayama-Yoshida, Jpn J Appl Phys **38**, L166 (1999)
61. Y. Dai, Y. Zhang, Q.K. Li, C.W. Nan, Chem Phys Lett **83**, 358 (2002)
62. K. Vanheusden, W.L. Warren, C.H. Seager, D.R. Tallant, J.A. Voigt, B.E. Gnade, J Appl Phys **79**, 7983 (1996)
63. M.H. Huang, Y. Wu, H. Feick, N. Tran, E. Weber, P. Yang, Adv Mater **13**, 113 (2001)
64. T. Tatsumi, M. Fujita, N. Kavamoto, M. Sasajima, Y. Horikoshi, J Appl Phys **43**, 2602 (2004)
65. B. Lin, Z. Fu, Y. Jia, Appl Phys Lett **79**, 943 (2001)